Phase-change nonlocal metasurfaces for dynamic wave-front manipulation

Tingting Liu,[1] Dandan Zhang,[2] Wenxing Liu,[2] Tianbao Yu,[2] Feng Wu,[3] Shuyuan Xiao,[1,*] Lujun Huang,[4,†] and Andrey E. Miroshnichenko[5,‡]

[1] *Institute for Advanced Study, Nanchang University, Nanchang 330031, China*
[2] *School of Physics and Materials Science, Nanchang University, Nanchang 330031, China*
[3] *School of Optoelectronic Engineering, Guangdong Polytechnic Normal University, Guangzhou 510665, China*
[4] *School of Physics and Electronic Sciences, East China Normal University, Shanghai 200241, China*
[5] *School of Engineering and Technology, University of New South Wales, Canberra ACT 2612, Australia*

(Received 15 January 2024; revised 10 March 2024; accepted 18 March 2024; published 1 April 2024)

Recent advances in nonlocal metasurfaces have enabled unprecedented success in shaping the wave front of light with spectral selectivity, offering alternative solutions for many emerging nanophotonics applications. The ability to tune both the spectral and spatial properties of such a class of metasurfaces is highly desirable, but the dynamic nonvolatile control remains elusive. Here, we demonstrate active narrowband wave-front manipulation by harnessing quasi-bound states in the continuum (quasi-BICs) in phase-change nonlocal metasurfaces. The proof-of-principle metasurfaces made of Sb_2S_3 allow for nonvolatile, reversible, and tunable spectral control over wave front and switchable spatial response at a given wavelength in the near-infrared regime. The design principle mainly builds upon the combination of the geometry phase of quasi-BICs and the dynamic tunability of phase-change meta-atoms to tailor the spatial response of light at tunable resonant wavelengths. By tuning the crystallization level of Sb_2S_3 meta-atoms through controlling the external stimuli, the dynamic nonlocal wave-front-shaping functionalities of beam steering, one-dimensional, and two-dimensional focusing, and holographic imaging are achieved exclusively at resonant wavelengths, with functionally transparent off resonance. This work represents a critical advance towards developing an integrated dynamic nonlocal metasurface for future augmented and virtual reality wearables.

DOI: 10.1103/PhysRevApplied.21.044004

I. INTRODUCTION

The past few decades have witnessed substantial progress of metasurfaces controlling the light field through subwavelength elements, as they can be designed with a variety of geometries and materials to generate a tailored optical response in terms of amplitude, phase, polarization, frequency, and other degrees of freedom [1–5]. Particularly with their ability to impart a specific phase profile using designed meta-atoms for wave-front control, metasurfaces have provided an elegant and fashionable strategy in miniaturizing and flattening optical systems [6–16]. The conventional metasurfaces are designed to imprint independent and spatially variant phases onto incident light waves, and these local devices would shape the wave front over a broad range of wavelengths due to the modulation as a function of position. However, in many emerging imaging, sensing, and display applications such as augmented reality (AR) and virtual reality (VR) systems, the functionalities that require highly localized energy and high spectral control over the wave front are inaccessible by the local metasurfaces. Most recently, several works have employed the concept of bound states in the continuum (BICs) to realize the nonlocal wave-front-shaping metasurfaces with large quality factor (Q factor) and spectral selectivity [17–21]. Based on the analysis of symmetry perturbations to the BICs, the general method for independently controlling local and nonlocal interaction of the metasurface supporting quasi-BICs is developed to shape the wave front by spatially varying the polarization properties of quasi-BICs only on resonance, leaving the nonresonant light unchanged. The nanostructures, such as wave-front-selective metasurface [22] and spectrally selective metalenses [23–25], have been theoretically and experimentally demonstrated, opening other pathways for future three-dimensional (3D) display platforms that complement those of conventional metasurfaces.

Despite the exciting advances in nonlocal metasurfaces, the ability to realize flat optical devices with controllable spectral and spatial response remains a significant

*Corresponding authors. syxiao@ncu.edu.cn
†ljhuang@phy.ecnu.edu.cn
‡andrey.miroshnichenko@unsw.edu.au

 © 2024 American Physical Society

ongoing challenge for practical applications. In previous works, researchers have realized the control of multiple quasi-BICs by adding successive symmetry-breaking perturbations to a single nonlocal metasurface, allowing for wave-front manipulation at several wavelengths [26,27]. In principle, up to four distinct functions from four quasi-BICs may be realized on a single metasurface though at the cost of denser patterning and increased crosstalk. Besides the single-layer structures, multiple nonlocal wave-front-shaping metasurfaces can also be stacked to mold the optical wave front distinctively at multiple wavelengths [25]. However, these approaches require delicate design and precise fabrication techniques. Moreover, such passive metasurfaces are designed to be static with fixed control over spatial and spectral response once they are fabricated. Inspired by the progress of tunable and reconfigurable nanophotonics [28–31], recent efforts have explored active tunability and reconfigurability of wave-front-shaping functionalities in nonlocal metasurfaces. For example, by leveraging tunable thermo-optic coefficient of titanium dioxide (TiO_2) material, the resonant wavelengths of quasi-BICs in TiO_2 nonlocal metasurface are thermally shifted through refractive-index tuning, and then the thermally switchable functionalities have been demonstrated in the metasurface [32]. In parallel, the spatial and spectral reconfigurability of nonlocal metasurfaces has also been explored in a mechanically stretchable deflector consisting of silicon pillars embedded in a stretchable polymer, where resonant wavelength and deflection angle can be simultaneously tunable via mechanical strain [33]. The thermally tunable and stretchable metasurfaces show the advantages of simple design, fabrication, and accessible tuning approaches. Nevertheless, once the thermal control or mechanical strain vanishes, the spectral and spatial responses of the metasurfaces recover to their initial states.

This work employs an emerging phase-change material, antimony trisulfide (Sb_2S_3), in nonlocal metasurfaces supporting quasi-BICs for dynamic spatial and spectral control in the near-infrared regime. By tuning the crystallization level of Sb_2S_3 using the appropriate external stimuli, such as thermal, electric, and optical excitations, wave-front shaping can be realized at tunable wavelengths, and the optical functionalities at specific wavelengths can be switched on to off. As a proof of concept, we design the Sb_2S_3 metasurface supporting the quasi-BIC that is evolved from the symmetry-protected BIC by the dimerization perturbation. The quasi-BIC obeys the selection rules, and the system is capable of shaping wave front only across the narrow spectral bandwidth of resonance using the geometric phase, while leaving the rest of the spectrum transparent. By tuning the crystallization level of Sb_2S_3 meta-atoms, the dynamic spectral and spatial control for functionalities, such as beam steering, cylindrical lensing, and radial lensing is theoretically designed and numerically demonstrated. Furthermore, the dynamic holographic imaging at distinct wavelengths is demonstrated, showing the great potential of the phase-change nonlocal metasurfaces in optical information storage and encryption. By introducing the meta-atoms made of the phase-change materials into the nonlocal wave-front-shaping metasurface, the active control of wave-front manipulation at narrow spectral bandwidth of the quasi-BIC resonances is realized with the advantage of multistate, reversible, and nonvolatile tunability in active nonlocal metasurfaces. It may lead to alternative device concepts and finding great potential in optical imaging, sensing, and display applications.

II. DESIGN PRINCIPLE

Figure 1 is a conceptual illustration of phase-change nonlocal metasurfaces enabling dynamic spatial control at distinct resonant wavelengths by tuning the crystallization level of Sb_2S_3. In the proposed metasurface, the wave-front manipulation stems from the geometric phase imparted onto the converted circularly polarized (CP) light of transmission mode on resonance. The geometric phase relies only on the polarization properties of quasi-BIC from symmetry breaking. Meanwhile, the quasi-BIC resonance of the metasurface strongly depends on the refractive index of Sb_2S_3 meta-atoms, which is tunable by adjusting the crystallization state of Sb_2S_3 through controlling the external stimulus including thermal, electric, and optical excitations [34–39]. Under the operating principle, dynamic wave-front manipulation can be realized at the wavelength-tunable resonance in a specific symmetry-broken quasi-BIC nanostructure. As shown in Fig. 1, the wave front would be shaped at the resonant wavelength when the broadband CP light illuminates onto the quasi-BIC metasurface with a designed phase profile. As Sb_2S_3 metasurface experiences phase transition from the amorphous (a-Sb_2S_3) to crystalline states (c-Sb_2S_3), the spectral response is shifted from λ_a to λ_c, tuning the centered wavelength of spatial control. Specifically, Sb_2S_3 material possesses multilevel nonvolatile tunable optical constants and the ultrafast reversible switching ability between the stable states. Benefiting from these advantages, the proposed Sb_2S_3 metasurfaces can realize dynamic, reversible, and nonvolatile wave-front manipulation at distinct wavelengths during the phase-transition process.

The proposed phase-change metasurfaces can manipulate the optical wave front by choosing a specific wavelength within a broad range, which is different from the previous nonlocal metasurfaces with only several target working wavelengths. This can be attributed to continuous spectral control over wave front in Sb_2S_3 metasurfaces. The proposed metasurface has more freedoms and higher security for information encryption. For example, the information decoding at a selected wavelength requires an appropriate stimulus to transform Sb_2S_3 into a given

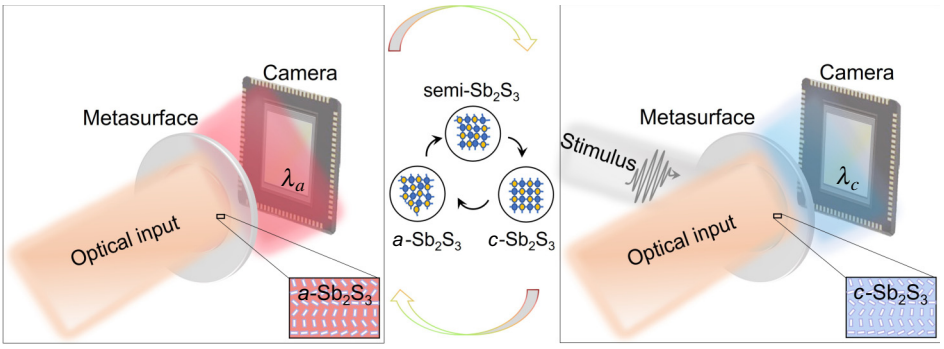

FIG. 1. Schematic diagram of dynamic wave-front manipulation at distinct wavelengths enabled by the proposed phase-change nonlocal metasurfaces. Using the Sb_2S_3 metasurface, the wave front of optical input is manipulated at the resonant wavelength of quasi-BIC. Through external stimuli, Sb_2S_3 meta-atom is phase changed between the amorphous (a-Sb_2S_3) and crystalline states (c-Sb_2S_3), leading to the resonant wavelength shifting between λ_a and λ_c. Inset in the middle is a generic scheme of the atomic distributions of the three crystallinity states, including a-Sb_2S_3, the intermediate state referred to semi-Sb_2S_3, and c-Sb_2S_3, which are nonvolatile stable states that can be reversibly switched during the phase-transition process. The resultant spectral shift of quasi-BIC resonance gives rise to a tunable center wavelength for the dynamic spatial response.

crystallization level, and misleading or useless information will be obtained either for other wavelengths or for other improper crystallization levels. Of note, it offers a solution for wearables and AR devices. For example, it can not only satisfy the need to shape optical wave front exclusively at selected wavelengths and leave the rest of the spectrum transparent but also bring the flexibility of adaptive control with tunable working wavelength of wave-front manipulation. The proposed metasurfaces offer a prototype for potential applications, such as information storage and encryption, AR and display technology.

To present the operation mechanism of the dynamic control of the spectral and spatial response, we first elucidate the evolution of the quasi-BIC resonance in the metasurface. BICs can be characterized as nonradiating resonant modes in an open system but without coupling to the radiating channels propagating outside the system [40–42]. Here we focus on the symmetry-protected BICs developed by symmetry-restricted coupling to free space. To be excitable from free space light for real applications, the leaky quasi-BICs with finite Q factors are induced by a symmetry-breaking perturbation. An alternative approach is the dimerization perturbation to double the period along the real-space dimension and halve the first Brillouin zone in momentum space. In Fig. 2(a), the simple structure comprising a rectangular aperture etched in a dielectric thin film is adopted for demonstration, with a dimerized meta-atom shown in Fig. 2(b). As compared in Figs. 2(c) and 2(d), the period-doubling perturbation effectively folds the band structure in the k space, such that the bound mode that was under the light line and not radiated to free space is folded into the continuum at the Γ point that can be excitable by free-space light under normal incidence. The existence of quasi-BIC resonance can also be confirmed by the broaden linewidth of transmission spectrum, as shown in the Supplemental Material [43]. In this evolution, the optical lifetime of such quasi-BIC can be controlled by the perturbation strength (δ) with Q factors varying inversely with δ as $Q \propto \delta^{-2}$, and the polarization properties are governed by selection rules specifying whether excitation of quasi-BIC is forbidden or allowed according to the space group of the perturbed symmetry [17,44–47]. Thus it is possible to attain the desired Q factor by adjusting the perturbation strength and realize the wave-front control by manipulating the polarization properties of quasi-BIC in a designed metasurface.

Then we consider the dimerized structure consisting of two rectangular holes in Sb_2S_3 thin film with a thickness of 150 nm on the silica substrate, as shown in Fig. 2(e). To concentrate on the dynamic wave-front control, the Q-factor engineering involved is not taken into consideration in the current work, and we set the constant symmetry-breaking strength of the structure with orthogonal holes with fixed length and width. Based on the selection rules [17], the dimerized structure is categorized as $p2$ space group. Independently of this optical localization and lifetime, the in-plane rotation angle α of the apertures controls the far-field polarization angle ϕ that can couple to the quasi-BIC mode, with a linear approximation of $\phi \approx 2\alpha$. This is derived from the parent-child symmetry relationship between higher-symmetry plane groups *pmm* and *pmg* as parent groups and $p2$ as the child group. The *pmm* parent space with $\alpha = 0^\circ$ allows mode coupling to x polarization with $\alpha = 0^\circ$, and *pmg* parent space with $\alpha = 45^\circ$ yields coupling to y polarization with $\phi = 90^\circ$. In other words, a continuous change of the in-plane rotation angle α from 0° to 45° leads to a 90° change in couplable polarization angle ϕ, leading to the $\phi \approx 2\alpha$ relationship. Like the conventional phase-gradient metasurface, the $p2$ space group system imparts the geometric phase to the converted CP

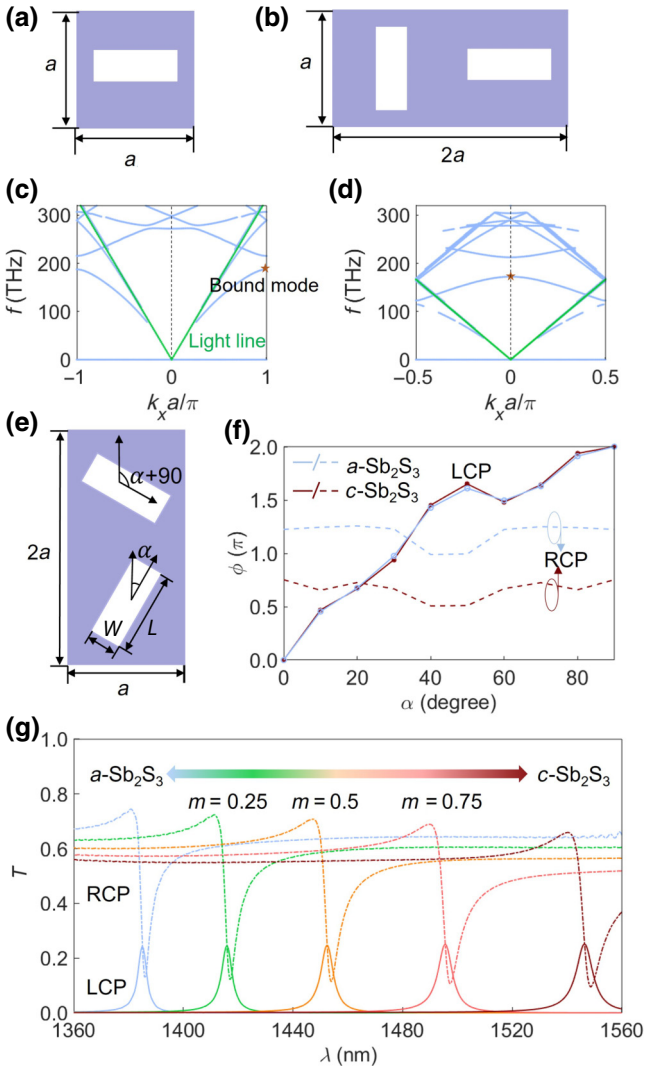

FIG. 2. The design of phase-change nonlocal metasurfaces. (a) The unperturbed meta-atom with a rectangular aperture etched in a thin film. (b) The dimerized meta-atom, with $a = 450$ nm, $L = 325$ nm, and $W = 125$ nm. (c),(d) The calculated band structures for meta-atoms in (a) and in (b), respectively. The green curve depicts the light line, and the star mark indicates the mode of interest. (e) The top view of the designed meta-atoms with rotation angles α. (f) The phase of converted LCP and unconverted RCP components in transmission for the a-Sb_2S_3 and c-Sb_2S_3 metasurfaces when the RCP is normally incident. (g) The simulated transmission spectra of the LCP and RCP components in transmission at different crystallization levels under the normal incidence of RCP.

light in transmission. Specifically, when the CP light is incident onto the metasurface, only the linear component in the polarization angle of $\phi_1 \approx 2\alpha$ completely coupling to the quasi-BIC, and subsequently, the linear polarized light on resonance is coupled out into the free space with decomposed CP component showing phase as $\phi_2 \approx 2\alpha$ for the converted part. Hence, the total geometric phase of the quasi-BIC in this process is derived as $\Phi = \phi_1 + \phi_2 \approx 4\alpha$ for the converted CP component, while the phase remains unchanged for the unconverted component due to the opposite signs canceling each other when transforming the linear and CP components. Such relations can be illustrated by Fig. 2(f). When the right-handed circularly polarized (RCP) light illuminates on the metasurfaces, the geometric phase of the transmitted light on quasi-BIC resonance shows an approximate relation of 4α for the converted component of LCP with a full phase coverage of $0 \sim 2\pi$, whereas the phase for the unconverted component of RCP is nearly unchanged.

Compared with the common phase-change material $Ge_2Sb_2Te_5$, Sb_2S_3 has a wide band gap of $1.7 \sim 2.05$ eV, showing much lower, even negligible absorption in the near-infrared regime of interest [34,39,48]. The refractive index of Sb_2S_3 can be adjusted from 2.8 to 3.5 in this regime (shown in Supplemental Material [43]). Via appropriate stimuli, including thermal, electric, and optical excitations, Sb_2S_3 can be switched reversibly and quickly between the amorphous (a-Sb_2S_3) and crystalline states (c-Sb_2S_3) or to be an intermediate state. Previous reports have demonstrated the full crystallization of the Sb_2S_3 nanostructures can be implemented in a furnace filled with argon (Ar) and held there for 1 h [34], and can also be realized with electrical and laser pulses in a more efficient way [35–39]. The order of the recrystallization switching speed for similar materials $Ge_2Sb_2Te_5$ by electrical means is approximately kHz [49]. The dielectric constant at different crystallization levels of Sb_2S_3 can be derived by the Lorenz-Lorentz relation as [49–52]

$$\frac{\varepsilon_{\text{eff}} - 1}{\varepsilon_{\text{eff}} + 2} = m\frac{\varepsilon_{\text{c}} - 1}{\varepsilon_{\text{c}} + 2} + (1 - m)\frac{\varepsilon_{\text{a}} - 1}{\varepsilon_{\text{a}} + 2}, \tag{1}$$

where m represents the crystalline fraction ranging from 0 to 1 for the intermediate state between a-Sb_2S_3 and c-Sb_2S_3, ε_a and ε_c are the permittivity of a-Sb_2S_3 and c-Sb_2S_3, respectively. Because of the tunable optical constants of meta-atoms, the spectral response of quasi-BIC in Sb_2S_3 metasurface will vary during these phase transitions. The numerical calculations are performed with the finite-difference-time-domain (FDTD) method via the ANSYS Lumerical Suit. As shown in Fig. 2(g), the transmission spectra show a shift of resonance wavelength within a broad band from approximately 1380 to approximately 1550 nm between a-Sb_2S_3 and c-Sb_2S_3 metasurfaces. For the converted light component of interest, namely, LCP, the peak transmission efficiencies of these spectra are always around the maximum theoretical limit of 0.25 in this four-port system [33]. In contrast with the spectral shift, the geometric phase of quasi-BIC on resonance mainly relying on the rotation angles is almost unchanged, as verified by that of the a-Sb_2S_3 and c-Sb_2S_3 metasurface in Fig. 2(f). A designer phase profile can be

realized at tunable wavelengths of quasi-BIC resonances. Of course, the wave-front-shaping ability in metasurfaces will be remarkably weakened at the nonresonance wavelengths due to the dramatically reduced transmission efficiency. This makes it possible to switch on and off the spatial response at a specific wavelength by transforming the resonant wavelength into nonresonant via varying the crystallization levels of Sb_2S_3. As a result, dynamic wave-front-shaping metasurface supporting a quasi-BIC can be implemented by a rational synthesis of multistate switchable spectral response in the Sb_2S_3 metasurface with a spatially varying geometric phase profile. Note that Sb_2S_3 is patterned into nanostructures to construct the nonlocal metasurface instead of the spacer layer in earlier works for active devices [53–56]. The nanofabrication techniques have been explored and proven to be feasible in previous experimental works [34,39], and the fabrication process for the proposed Sb_2S_3 metasurface is illustrated in the Supplemental Material [43].

III. RESULTS AND DISCUSSION

Using the dimerized Sb_2S_3 meta-atoms with different rotation angles for specific phase profiles, wavelength-tunable spectral control over wave-front and switchable spatial response at a selected wavelength can be realized, creating active metadevices, such as beam deflectors and lenses. For demonstration, we start from a common wave-front-shaping function of anomalous refraction for beam steering. According to the generalized Snell's law [6,7], the nonlocal wave-front-shaping metasurface with a gradient distribution of rotation angle is devised, as shown in Fig. 3(a). The Sb_2S_3 meta-atoms are spatially arranged for one period of the metasurface with varying α at each position to linearly grade the corresponding geometric phase along the direction orthogonal to the dimerization, but with constant aperture dimensions and lattice constants. When RCP light is normally incident from the substrate side of the metasurface, the transmission spectra for the converted LCP and unconverted RCP component are presented in Fig. 3(b). As the crystallization fraction m of Sb_2S_3 material changes from 0 to 1, namely from a-Sb_2S_3 to c-Sb_2S_3, the resonance wavelength of quasi-BIC shows a continous redshift across a wavelength regime of approximately 160 nm. Here, we select the intermediate state with $m = 0.5$ as the semicrystalline state of Sb_2S_3 (semi-Sb_2S_3) to demonstrate the continuous control.

As a consequence of the tunable wavelength of quasi-BIC resonance, the metasurface is able to perform wave-front shaping at different wavelengths. As shown in Fig. 3(c), the converted LCP component is refracted to 14° at resonance wavelength of 1381 nm for a-Sb_2S_3, 15° at 1450 nm for semi-Sb_2S_3, and 16° at 1545 nm for c-Sb_2S_3, respectively. At these corresponding resonance wavelengths, approximately 20% of the light is removed from the incident beam and redirected into the second-order diffracted beam [26]. Meanwhile, no deflection for the unconverted RCP component can be observed in Fig. 3(c) due to the constant phase profiles. Unlike the conventional phase-gradient metasurfaces, the designed metasurface using resonant meta-atoms shapes the wave front of the converted LCP component only at resonance. Such nonlocal wave-front-shaping ability can be verified by comparing the field distributions of an arbitrary nonresonant wavelength at 1500 nm (shown in the Supplemental Material [43]) and the respective resonant wavelengths. The phase-change metasurface demonstrates the dynamic beam deflection for the converted LCP transmission light at distinct resonant wavelengths while remaining unchanged for unconverted RCP or nonresonance.

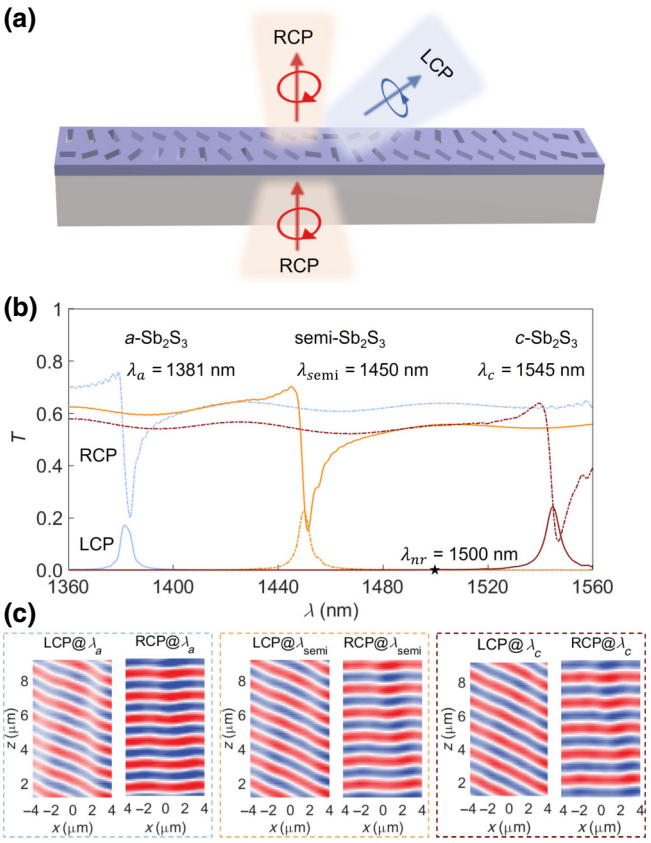

FIG. 3. The design of phase-change nonlocal metasurfaces for dynamic beam steering at distinct wavelengths. (a) The schematic diagram of a superunit cell of the dynamic beam deflector consisting of 25 dimerized meta-atoms with spatially varying rotation angles α from 0 to π. (b) The transmission spectra of the nonlocal metasurface at different crystallization states of a-Sb_2S_3, semi-Sb_2S_3, and c-Sb_2S_3 for RCP and LCP components under normal RCP incidence. (c) The electric filed profiles for RCP and LCP components at the corresponding resonant wavelengths of a-Sb_2S_3, semi-Sb_2S_3, and c-Sb_2S_3 metasurfaces, showing the active beam deflection at tunable wavelengths of quasi-BIC resonances for converted LCP component.

Next we consider simple cylindrical metalens for dynamic narrowband focusing, as shown in Fig. 4(a). Under the normally incident RCP light, the transmitted LCP light is focused to a specific distance at tunable wavelengths by varying crystallization state of Sb_2S_3. The typical phase profile of the metalens with focal length f is given by [57–60]

$$\phi_r = \frac{2\pi}{\lambda_0}(\sqrt{r^2 + f^2} - f), \tag{2}$$

where $r = \sqrt{x^2 + y^2}$ is the distance from arbitrary position (x, y), and λ_0 is the target working wavelength. Here, the one-dimensional metalens for space light focusing is designed, where the meta-atoms with a specific phase profile shown in Fig. 4(b) are arranged along the x direction from -22.5 to 22.5 μm. The focal length of the metalens is 100 μm, and the working wavelength is set as the same as the resonant wavelength for a-Sb_2S_3 metasurface. The spatially varying phase profile is coded by Sb_2S_3 meta-atoms with different rotation angles α at corresponding coordinate, according to the nearly linear dependence of the geometric phase on the rotation angle of $\Phi \approx 4\alpha$.

In Fig. 4(c), the transmission spectra of the cylindrical metalens demonstrate that the converted LCP light shows a peak at resonant wavelength, and the resonance peak can be shifted from approximately 1380 to approximately 1550 nm by varying the crystallization state of phase-change meta-atoms from a-Sb_2S_3 to c-Sb_2S_3. Similarly, the resonant wavelength shift for different Sb_2S_3 contributes to the tunable spatial and spectral response. Figure 4(d) illustrates the normalized intensity of the converted LCP light fields at the corresponding resonant wavelength of a-Sb_2S_3, semi-Sb_2S_3, and c-Sb_2S_3, respectively. Since the geometric phase is fundamentally robust, the light fields at these wavelengths are all focused, implying the ability of spatial control at continous wavelengths within a broad spectral range. For a selected wavelength, the focusing effect can be switched on-to-off by tuning the resonant position of quasi-BIC. The focusing intensity of fields shows an observable increase, accompanied by the increasing transmission peak when the meta-atoms phase changed from a-Sb_2S_3 to c-Sb_2S_3. This can be explained by the fact that the relatively larger refractive index of c-Sb_2S_3 and negligible loss account for a stronger localized light field and, thus, stronger spatial control ability. In contrast with the space light focusing of the converted LCP component, the wave-front shaping is not performed for the unconverted RCP component in Fig. 4(d) and the nonresonant wavelengths, for example, at $\lambda = 1500$ nm (shown in the Supplemental Material [43]).

We proceed to the more complex two-dimensional (2D) spatial control at distinct resonant wavelengths of quasi-BICs. The phase-change metasurface for a radial lens is designed in a simple-to-implement way, which focuses the

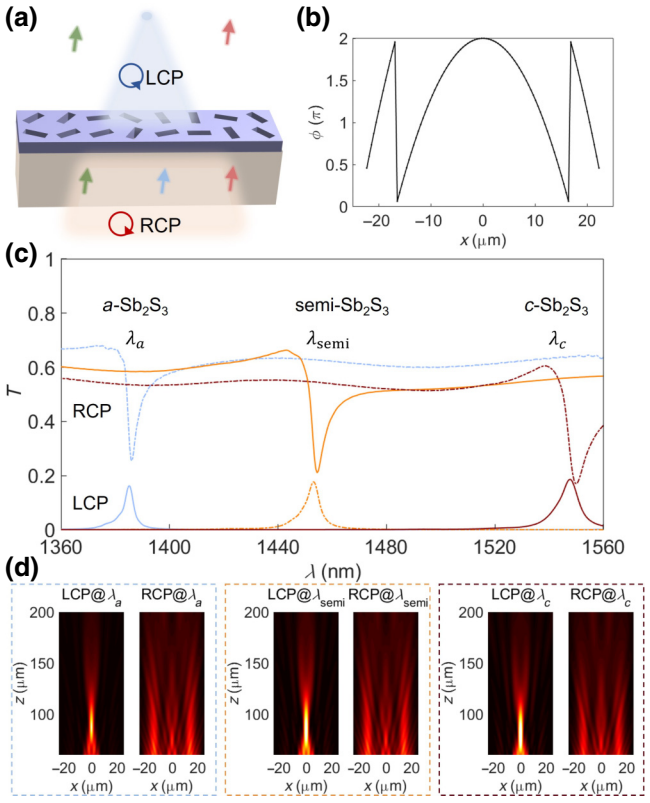

FIG. 4. The design of phase-change metasurfaces for dynamic cylindrical metalens at distinct wavelengths. (a) The schematic diagram of the dynamic narrowband focusing along x direction. (b) The phase profile of the 1D focuses on the converted LCP. (c) The transmission spectra of the nonlocal metasurface at different crystallization states. (d) The far-field intensity distributions near the designed focal spot of 100 μm for RCP and LCP component at the corresponding resonant wavelengths of a-Sb_2S_3, semi-Sb_2S_3, and c-Sb_2S_3 metasurfaces, showing the space light focusing at tunable wavelengths of quasi-BIC resonances for converted LCP component.

transmitted LCP component into a specific spot in space, as shown in Fig. 5(a). The spatial phase profile from Eq. (1) is presented in Fig. 5(b) with a 2D distribution dependent on the coordinate x and y. The light focusing with focal spots imaging at the focal plane occurs only when the incident wavelengths tune around the quasi-BIC resonance. As the geometric phase of $\Phi \approx 4\alpha$ is imparted onto the transmitted LCP component on quasi-BIC resonances, the phase profile can be encoded by the 2D spatial distribution of Sb_2S_3 meta-atoms with corresponding rotation angle α. Here, a nonlocal radial metalens with a diameter of 30 μm is designed and it has an initial working wavelength centered at the resonant wavelength for the a-Sb_2S_3 metasurface.

The transmission spectra of the designed metasurface for different crystallization states of Sb_2S_3 are depicted in Fig. 5(c). Compared with those of beam deflection

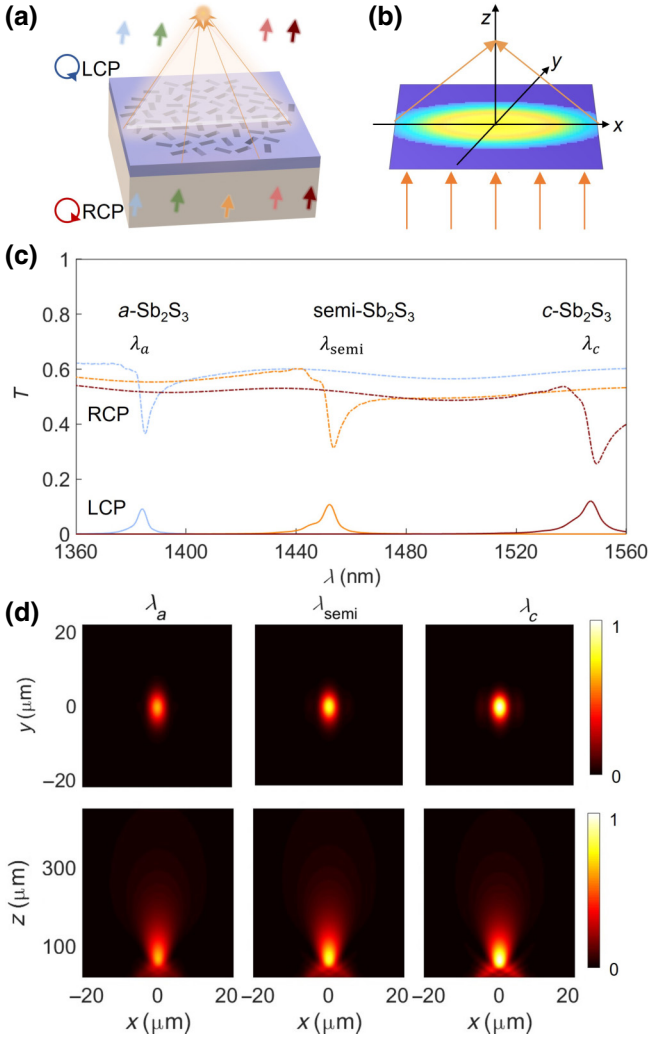

FIG. 5. The design of phase-change metasurfaces for dynamic radial metalens at distinct wavelengths. (a) The schematic diagram of the dynamic narrowband focusing in 2D space. (b) The spatial phase profile for the 2D focusing. (c) The transmission spectra of the phase-change nonlocal metasurfaces at different crystallization states. (d) The transverse far-field profiles on the focal plane and the longitudinal far-field profiles through the focal spot, for the converted LCP component at the corresponding resonant wavelengths of a-Sb_2S_3, semi-Sb_2S_3, and c-Sb_2S_3 metasurfaces.

metasurface and the cylindrical metalens above, the resonances remain intact even through the various geometry in these metadevices. This implies that the quasi-BIC resonance has a relatively stable resonance wavelength and peak amplitude for the various combinations of specific meta-atoms either in 1D or 2D. Such robustness would benefit the metadevice design where the spectral response can be defined by designing a single unit cell. The transverse and longitudinal far-field distributions with the focal spots on the quasi-BIC resonances in Fig. 5(d) show the efficient focusing ability at the corresponding resonant wavelength of different Sb_2S_3 metasurfaces. The relatively larger focusing intensity of the c-Sb_2S_3 metasurface can be attributed to the increasing refractive index during the crystallization process. In addition, the focal spots off resonance for c-Sb_2S_3 show the efficiency decreasing as the wavelengths gradually move away from the center of the resonance (shown in the Supplemental Material [43]). With several orders of magnitude smaller power at off-resonance wavelengths than background plane wave, the metalens can be considered functionally transparent off resonance. Such spectral selectivity to the crystallization state of Sb_2S_3 leads to the tunability to either manipulate wave front at a controllable wavelength or switch on and off the function at a selected wavelength.

In the proposed phase-change nonlocal metasurface, the flexibility to control both the spatial and spectral response can provide abundant degrees of freedom for implementing the narrowband wave-front manipulation in various applications associated with optical information processing. To demonstrate the versatility and high performance, a phase-only metahologram is finally designed. Using the same meta-atom library with the lenses above, the information is coded by the geometric phases of Sb_2S_3 meta-atoms that are exerted to the transmitted converted component on resonance. Here, the phase profile of the image is obtained by the Gerchberg-Saxton algorithm and then encoded by the 2D spatial distribution of the rotation angle of Sb_2S_3 meta-atoms.

The simulated diffraction patterns shown in Fig. 6 are generated by the a-Sb_2S_3, semi-Sb_2S_3, and c-Sb_2S_3, respectively. For comparison, the holographic images at resonant and nonresonant wavelengths are presented. Before the phase transition of Sb_2S_3 meta-atoms, namely a-Sb_2S_3 metasurface, the image is only captured for the converted LCP light at the corresponding resonant wavelength around 1380 nm, while no image displays at the other two nonresonant wavelengths. Similar results can be observed for the semi-Sb_2S_3 and c-Sb_2S_3 metasurfaces. Such a mapping relationship in the space-wavelength domains for holographic imaging originated from the fact that the geometric phase profiles in the metasurface are fundamentally robust at different resonant wavelengths, with the correlated rotation angles of meta-atoms hardly affecting the spectral response. These significant properties can be applied to optical information encryption where the information decryption requires the matching conditions between the selected wavelength and the appropriate crystallization level of Sb_2S_3 meta-atoms. Of note, the proposed metasurface attempts to develop the optical metadevice capable of performing dynamic operations on incident light waves with high degrees of spectral control. The proposed metasurface allows the transmitted information only at selected narrowband wavelengths to be processed, avoiding the extra optical components such as polarizers to add the size and mass of system. It can also

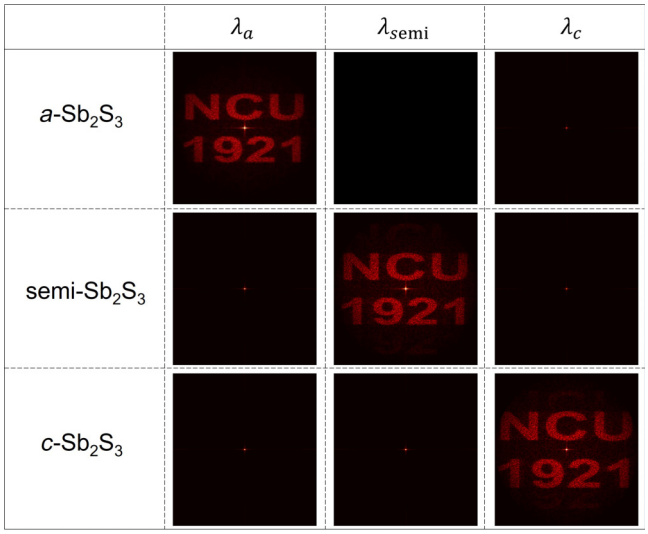

FIG. 6. The demonstrations of dynamic spatial and spectral control in the phase-change nonlocal metasurfaces using a phase-only metahologram. Under RCP illumination, the diffraction patterns generated by the a-Sb_2S_3, semi-Sb_2S_3, and c-Sb_2S_3 metasurfaces of transmitted LCP component display images exclusively at selected wavelengths, and display misleading or useless information for the nonresonant regime.

achieve an adaptive selection of the operating wavelength across a broad spectral bandwidth for information imaging, display, and sensing.

IV. CONCLUSIONS

In conclusion, we have demonstrated phase-change nonlocal metasurfaces capable of actively shaping light's spatial and spectral properties in transmission mode. The functionality is enabled by incorporating the phase-change meta-atoms integrated with a nonlocal wave-front-shaping metasurface empowered by quasi-BICs. A systematic design approach is presented by combining the nonlocal design strategies of enhanced light-matter interaction of quasi-BICs and the wave-front-shaping principle encapsulated by the generalized Snell's law in the phase-change metasurfaces. Leveraging spatially varying the polarization properties of quasi-BICs for designer geometric phase profiles, the wave-front-shaping functions for beam steering and space focusing are demonstrated for a narrow spectral regime in Sb_2S_3 metasurfaces. By switching the state of Sb_2S_3 between amorphous and crystalline, the wave-front manipulation can be realized at multiwavelength within a broad spectral range, and the spatial response at a specific wavelength can be switched on to off. The presented Sb_2S_3 metasurface platform can afford multistate, reversible, and nonvolatile tuning of the spatial and spectral response, offering sufficient design freedom to tailor the spatial response at tunable wavelength actively. Furthermore, the dynamic control over a single device's spatial and spectral response enables holographic imaging at selected wavelengths, which may open the door for next-generation compact narrowband imaging for applications, such as information storage and encryption and AR and VR.

ACKNOWLEDGMENTS

This work was supported by the National Natural Science Foundation of China (Grants No. 12364045, No. 12304420, No. 12264028, and No. 12104105), the Natural Science Foundation of Jiangxi Province (Grants No. 20232BAB211025 and No. 20232BAB201040), the Chenguang Program of Shanghai Education Development Foundation and Shanghai Municipal Education Commission (Grant No. 21CGA55), the Shanghai Pujiang Program (Grant No. 22PJ1402900), the Guangdong Basic and Applied Basic Research Foundation (Grant No. 2023A1515011024), the Science and Technology Program of Guangzhou (Grant No. 202201011176), the Young Elite Scientists Sponsorship Program by JXAST (Grant No. 2023QT11), the China Scholarship Council (Grant No. 202008420045), and the Australian Research Council Discovery Project (Grant No. DP200101353).

[1] A. V. Kildishev, A. Boltasseva, and V. M. Shalaev, Planar photonics with metasurfaces, Science **339**, 1232009 (2013).
[2] N. Yu and F. Capasso, Flat optics with designer metasurfaces, Nat. Mater. **13**, 139 (2014).
[3] F. Ding, A. Pors, and S. I. Bozhevolnyi, Gradient metasurfaces: A review of fundamentals and applications, Rep. Prog. Phys. **81**, 026401 (2017).
[4] S. So, J. Mun, J. Park, and J. Rho, Revisiting the design strategies for metasurfaces: Fundamental physics, optimization, and beyond, Adv. Mater. **35**, 2206399 (2023).
[5] A. Arbabi and A. Faraon, Advances in optical metalenses, Nat. Photonics **17**, 16 (2022).
[6] N. Yu, P. Genevet, M. A. Kats, F. Aieta, J.-P. Tetienne, F. Capasso, and Z. Gaburro, Light propagation with phase discontinuities: Generalized laws of reflection and refraction, Science **334**, 333 (2011).
[7] S. Sun, Q. He, S. Xiao, Q. Xu, X. Li, and L. Zhou, Gradient-index meta-surfaces as a bridge linking propagating waves and surface waves, Nat. Mater. **11**, 426 (2012).
[8] W. T. Chen, A. Y. Zhu, V. Sanjeev, M. Khorasaninejad, Z. Shi, E. Lee, and F. Capasso, A broadband achromatic metalens for focusing and imaging in the visible, Nat. Nanotechnol. **13**, 220 (2018).
[9] R. J. Lin, V.-C. Su, S. Wang, M. K. Chen, T. L. Chung, Y. H. Chen, H. Y. Kuo, J.-W. Chen, J. Chen, Y.-T. Huang, J.-H. Wang, C. H. Chu, P. C. Wu, T. Li, Z. Wang, S. Zhu, and D. P. Tsai, Achromatic metalens array for full-colour light-field imaging, Nat. Nanotechnol. **14**, 227 (2019).
[10] Z. Li, C. Chen, Z. Guan, J. Tao, S. Chang, Q. Dai, Y. Xiao, Y. Cui, Y. Wang, and S. Yu *et al.*, Three-channel

metasurfaces for simultaneous meta-holography and meta-nanoprinting: A single-cell design approach, Laser Photonics Rev. **14**, 2000032 (2020).
[11] P. Georgi, Q. Wei, B. Sain, C. Schlickriede, Y. Wang, L. Huang, and T. Zentgraf, Optical secret sharing with cascaded metasurface holography, Sci. Adv. **7**, eabf9718 (2021).
[12] Y. Guo, S. Zhang, M. Pu, Q. He, J. Jin, M. Xu, Y. Zhang, P. Gao, and X. Luo, Spin-decoupled metasurface for simultaneous detection of spin and orbital angular momenta via momentum transformation, Light Sci. Appl. **10**, 63 (2021).
[13] X. Luo, Y. Hu, X. Ou, X. Li, J. Lai, N. Liu, X. Cheng, A. Pan, and H. Duan, Metasurface-enabled on-chip multiplexed diffractive neural networks in the visible, Light Sci. Appl. **11**, 158 (2022).
[14] H. Ren, X. Fang, J. Jang, J. Bürger, J. Rho, and S. A. Maier, Complex-amplitude metasurface-based orbital angular momentum holography in momentum space, Nat. Nanotechnol. **15**, 948 (2020).
[15] S. Li and C. W. Hsu, Thickness bound for nonlocal wide-field-of-view metalenses, Light Sci. Appl. **11**, 338 (2022).
[16] S. Li and C. W. Hsu, Transmission efficiency limit for nonlocal metalenses, Laser Photonics Rev. **17**, 2300201 (2023).
[17] A. C. Overvig, S. C. Malek, M. J. Carter, S. Shrestha, and N. Yu, Selection rules for quasibound states in the continuum, Phys. Rev. B **102**, 035434 (2020).
[18] D. Sang, M. Xu, Q. An, and Y. Fu, Broadband transparent and high-Q resonant polarization meta-grating enabled by a non-local geometric-phase metasurface, Opt. Express **30**, 26664 (2022).
[19] A. Overvig, Y. Kasahara, G. Xu, and A. Alù, Demonstration of a polarization-agnostic geometric phase in nonlocal metasurfaces, arXiv:2302.13215.
[20] H. Huang, A. C. Overvig, Y. Xu, S. C. Malek, C.-C. Tsai, A. Alù, and N. Yu, Leaky-wave metasurfaces for integrated photonics, Nat. Nanotechnol. **18**, 580 (2023).
[21] G. Xu, A. Overvig, Y. Kasahara, E. Martini, S. Maci, and A. Alù, Arbitrary aperture synthesis with nonlocal leaky-wave metasurface antennas, Nat. Commun. **14**, 4380 (2023).
[22] A. Overvig and A. Alù, Wavefront-selective Fano resonant metasurfaces, Adv. Photonics **3**, 026002 (2021).
[23] A. Overvig and A. Alù, Diffractive nonlocal metasurfaces, Laser Photonics Rev. **16**, 2100633 (2022).
[24] R. Chen, T. Li, Q. Bi, S. Wang, S. Zhu, and Z. Wang, Quasi-bound states in the continuum-based switchable light-field manipulator, Opt. Mater. Express **12**, 1232 (2022).
[25] S. C. Malek, A. C. Overvig, A. Alù, and N. Yu, Multifunctional resonant wavefront-shaping meta-optics based on multilayer and multi-perturbation nonlocal metasurfaces, Light Sci. Appl. **11**, 246 (2022).
[26] A. C. Overvig, S. C. Malek, and N. Yu, Multifunctional nonlocal metasurfaces, Phys. Rev. Lett. **125**, 017402 (2020).
[27] Y. Zhou, S. Guo, A. C. Overvig, and A. Alù, Multiresonant nonlocal metasurfaces, Nano Lett. **23**, 6768 (2023).
[28] F. Ding, Y. Yang, and S. I. Bozhevolnyi, Dynamic metasurfaces using phase-change chalcogenides, Adv. Opt. Mater. **7**, 1801709 (2019).
[29] S. Xiao, T. Wang, T. Liu, C. Zhou, X. Jiang, and J. Zhang, Active metamaterials and metadevices: A review, J. Phys. D: Appl. Phys. **53**, 503002 (2020).
[30] J. Kim, J. Seong, Y. Yang, S.-W. Moon, T. Badloe, and J. Rho, Tunable metasurfaces towards versatile metalenses and metaholograms: A review, Adv. Photonics **4**, 024001 (2022).
[31] O. A. M. Abdelraouf, Z. Wang, H. Liu, Z. Dong, Q. Wang, M. Ye, X. R. Wang, Q. J. Wang, and H. Liu, Recent advances in tunable metasurfaces: Materials, design, and applications, ACS Nano **16**, 13339 (2022).
[32] S. C. Malek, C.-C. Tsai, and N. Yu, Thermally-switchable metalenses based on quasi-bound states in the continuum, arXiv:2306.13644.
[33] S. C. Malek, A. C. Overvig, S. Shrestha, and N. Yu, Active nonlocal metasurfaces, Nanophotonics **10**, 655 (2021).
[34] L. Lu, Z. Dong, F. Tijiptoharsono, R. J. H. Ng, H. Wang, S. D. Rezaei, Y. Wang, H. S. Leong, P. C. Lim, and J. K. Yang *et al.*, Reversible tuning of Mie resonances in the visible spectrum, ACS Nano **15**, 19722 (2021).
[35] Z. Fang, J. Zheng, A. Saxena, J. Whitehead, Y. Chen, and A. Majumdar, Non-volatile reconfigurable integrated photonics enabled by broadband low-loss phase change material, Adv. Opt. Mater. **9**, 202002049 (2021).
[36] O. Hemmatyar, S. Abdollahramezani, I. Zeimpekis, S. Lepeshov, A. Krasnok, A. I. Khan, K. M. Neilson, C. Teichrib, T. Brown, and E. Pop *et al.*, Enhanced meta-displays using advanced phase-change materials, arXiv:2107.12159.
[37] M. Delaney, I. Zeimpekis, D. Lawson, D. W. Hewak, and O. L. Muskens, A new family of ultralow loss reversible phase-change materials for photonic integrated circuits: Sb_2S_3 and Sb_2Se_3, Adv. Funct. Mater. **30**, 2002447 (2020).
[38] K. Gao, K. Du, S. Tian, H. Wang, L. Zhang, Y. Guo, B. Luo, W. Zhang, and T. Mei, Intermediate phase-change states with improved cycling durability of Sb_2S_3 by femtosecond multi-pulse laser irradiation, Adv. Funct. Mater. **31**, 2103327 (2021).
[39] P. Moitra, Y. Wang, X. Liang, L. Lu, A. Poh, T. W. Mass, R. E. Simpson, A. I. Kuznetsov, and R. Paniagua-Dominguez, Programmable wavefront control in the visible spectrum using low-loss chalcogenide phase-change metasurfaces, Adv. Mater. **35**, 2205367 (2022).
[40] C. W. Hsu, B. Zhen, A. D. Stone, J. D. Joannopoulos, and M. Soljačić, Bound states in the continuum, Nat. Rev. Mater. **1**, 16048 (2016).
[41] A. F. Sadreev, Interference traps waves in an open system: Bound states in the continuum, Rep. Prog. Phys. **84**, 055901 (2021).
[42] L. Huang, L. Xu, D. A. Powell, W. J. Padilla, and A. E. Miroshnichenko, Resonant leaky modes in all-dielectric metasystems: Fundamentals and applications, Phys. Rep. **1008**, 1 (2023).
[43] See Supplemental Material at http://link.aps.org/supplemental/10.1103/PhysRevApplied.21.044004 for the refractive index of Sb_2S_3; the simulation methods; the transmission spectrum for quasi-BIC; the fabrication procedure of the nanostructured Sb_2S_3 metasurface; the nonlocal wave-front shaping of the proposed beam deflection metasurface; the nonlocal 1D focusing of the proposed radial metalens; the narrowband spatial focusing of the proposed cylindrical metalens.

[44] K. Koshelev, S. Lepeshov, M. Liu, A. Bogdanov, and Y. Kivshar, Asymmetric metasurfaces with high-Q resonances governed by bound states in the continuum, Phys. Rev. Lett. **121**, 193903 (2018).

[45] S. Li, C. Zhou, T. Liu, and S. Xiao, Symmetry-protected bound states in the continuum supported by all-dielectric metasurfaces, Phys. Rev. A **100**, 063803 (2019).

[46] X. Wang, J. Duan, W. Chen, C. Zhou, T. Liu, and S. Xiao, Controlling light absorption of graphene at critical coupling through magnetic dipole quasi-bound states in the continuum resonance, Phys. Rev. B **102**, 155432 (2020).

[47] S. Xiao, M. Qin, J. Duan, F. Wu, and T. Liu, Polarization-controlled dynamically switchable high-harmonic generation from all-dielectric metasurfaces governed by dual bound states in the continuum, Phys. Rev. B **105**, 195440 (2022).

[48] L. Lu, S. Reniers, Y. Wang, Y. Jiao, and R. E. Simpson, Reconfigurable InP waveguide components using the Sb_2S_3 phase change material, J. Opt. **9**, 094001 (2022).

[49] S. Abdollahramezani, O. Hemmatyar, M. Taghinejad, H. Taghinejad, A. Krasnok, A. A. Eftekhar, C. Teichrib, S. Deshmukh, M. A. El-Sayed, E. Pop, M. Wuttig, A. Alù, W. Cai, and A. Adibi, Electrically driven reprogrammable phase-change metasurface reaching 80% efficiency, Nat. Commun. **13**, 1696 (2022).

[50] J. Tian, H. Luo, Y. Yang, F. Ding, Y. Qu, D. Zhao, M. Qiu, and S. I. Bozhevolnyi, Active control of anapole states by structuring the phase-change alloy $Ge_2Sb_2Te_5$, Nat. Commun. **10**, 396 (2019).

[51] Q. Meng, X. Chen, W. Xu, Z. Zhu, X. Yuan, and J. Zhang, High q resonant Sb_2S_3-lithium niobate metasurface for active nanophotonics, Nanomaterials **11**, 2373 (2021).

[52] T. Liu, Z. Han, J. Duan, and S. Xiao, Phase-change metasurfaces for dynamic image display and information encryption, Phys. Rev. Appl. **18**, 044078 (2022).

[53] S.-Y. Lee, Y.-H. Kim, S.-M. Cho, G. H. Kim, T.-Y. Kim, H. Ryu, H. N. Kim, H. B. Kang, C.-Y. Hwang, and C.-S. Hwang, Holographic image generation with a thin-film resonance caused by chalcogenide phase-change material, Sci. Rep. **7**, 41152 (2017).

[54] H. Zhou, Y. Wang, X. Li, Q. Wang, Q. Wei, G. Geng, and L. Huang, Switchable active phase modulation and holography encryption based on hybrid metasurfaces, Nanophotonics **9**, 905 (2020).

[55] L. Mao, Y. Li, G. Li, S. Zhang, and T. Cao, Reversible switching of electromagnetically induced transparency in phase change metasurfaces, Adv. Photonics **2**, 056004 (2020).

[56] T. Liu, X. Fang, and S. Xiao, Tuning nonlinear second-harmonic generation in AlGaAs nanoantennas via chalcogenide phase-change material, Phys. Rev. B **104**, 195428 (2021).

[57] X. Chen, L. Huang, H. Mühlenbernd, G. Li, B. Bai, Q. Tan, G. Jin, C.-W. Qiu, S. Zhang, and T. Zentgraf, Dual-polarity plasmonic metalens for visible light, Nat. Commun. **3**, 1198 (2012).

[58] M. Khorasaninejad, W. T. Chen, R. C. Devlin, J. Oh, A. Y. Zhu, and F. Capasso, Metalenses at visible wavelengths: Diffraction-limited focusing and subwavelength resolution imaging, Science **352**, 1190 (2016).

[59] M. Zhao, M. K. Chen, Z.-P. Zhuang, Y. Zhang, A. Chen, Q. Chen, W. Liu, J. Wang, Z.-M. Chen, B. Wang, X. Liu, H. Yin, S. Xiao, L. Shi, J.-W. Dong, J. Zi, and D. P. Tsai, Phase characterisation of metalenses, Light Sci. Appl. **10**, 52 (2021).

[60] J. Li, J. Li, Z. Yue, C. Zheng, G. Wang, J. Liu, H. Xu, C. Song, F. Yang, H. Li, F. Li, T. Tang, Y. Zhang, Y. Zhang, and J. Yao, Structured vector field manipulation of terahertz wave along the propagation direction based on dielectric metasurfaces, Laser Photonics Rev. **16**, 2200325 (2022).